Reduction of Conducted Interference by Steel Armor in Buried Cables: Measurements and Modeling

H. Tjerk Steenstra and Alexander P. J. van Deursen, *Senior Member, IEEE*

***Abstract*—Switched-mode power supplies in variable-frequency drives often combine good electrical efficiency with generous production of conducted emission. The common-mode (CM) current through the output-to-motor cable may perturb nearby systems via cable-to-cable crosstalk. Parameters relevant for the coupling are the rise–fall times and amplitude of the output current and voltage, and types and lengths of the cables. Of the many techniques to reduce the crosstalk, we investigated a particular one: reduction of the CM current by the armor of the motor cable. The armor is intended for mechanical protection, but may also substantially reduce the crosstalk. In an actual installation, we measured the transient current through the three phase leads of a motor cable. The cable length was 85 m, and it was buried in wet soil for most of its length. We also measured the transfer impedance of the armor up to 10 MHz, and used this to calculate the overall CM current in a coupled cable model using assumed reasonable values for the cable and soil parameters. Measurements and model results agreed well on the amplitude of the dominant resonance at about 300 kHz. The ratio of the inside transients to CM current was a factor of 20.**

***Index Terms*—Cable shielding, coupled transmission lines, electromagnetic compatibility, grounding, switched mode power supplies.**

I. Introduction

IN A MAJOR project to establish proper electromagnetic compatibility (EMC) measures in large industrial installations [1], we want to come up with a database of tested models for the design of large industrial electrotechnical installations with proper attention paid to EMC. It is desirable to put on all available metal for purposes of EMC in order to improve the cost/benefit ratio. This paper presents an example of a realized installation, where we predict *a posteriori* the conducted emission from a variable-frequency drive for an induction motor.

The model is based on the available parameters or those that can be obtained from practical experience, and parameters provided by additional dedicated measurements such as the transfer impedance of the cable. The aim is to assess the reduction of the conducted emission by the steel armor of a V0-YMvKas cable used as a shield. The code "V0-YMvKas," describing the cable, is explained in detail in [2]. The armor is primarily intended for protection against mechanical damage, such as intrusion of spades. Of course, shielded cables exist with much better performance. But still, the reduction by the armor is large enough not to be wasted.

Fig. 1. Trench with dozens of cables.

The installation is a part of the waste-water purification plant "Dongemond" located in Oosterhout (The Netherlands). The drives were installed in a control kiosk, and cables of the order of 100-m-long connected drives and motors. The cables were buried in wet soil over most of their length (see Fig. 1). Safety regulations required armored cables outdoor. The armors were treated as if they were a shield. Following good installation practice [3], the cable armor was clamped by a bracket to the grounded bare metal base plate on which the drive was mounted. At the motor end of the cable, a gland connected the armor to the motor chassis over the full armor circumference.

The switched-mode 7.5-kW variable-frequency drive generates three-phase 400-V pulsewidth-modulated signals at 3 kHz switching frequency. The motor has its windings in the usual delta configuration. The connection between the drive and this motor is an 85-m-long V0-YMvKas cable with four 6-mm^2

Manuscript received June 25, 2007; revised February 27, 2008. This work was supported by the Dutch Ministry of Economic Affairs' Innovative Research Project Program under the Electro Magnetic Power Technique (EMVT) Project 2301A.

H. T. Steenstra was with the Department of Electrical Engineering, Mathematics, and Computer Science, Delft University of Technology, 2600 AA Delft, The Netherlands. He is now with Mapper Lithography, 2628 XK Delft, The Netherlands (e-mail: tjerk.steenstra@mapperlithography.com).

A. P. J. van Deursen is with the Department of Electrical Engineering, Eindhoven University of Technology, 5612 AZ Eindhoven, The Netherlands (e-mail: a.p.j.v.deursen@tue.nl).

Color versions of one or more of the figures in this paper are available online at http://ieeexplore.ieee.org.

Digital Object Identifier 10.1109/TEMC.2008.926902

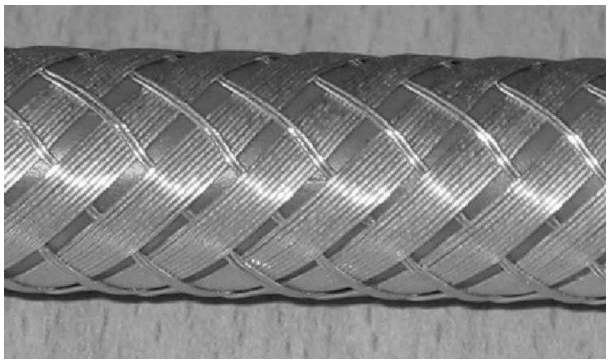

Fig. 2. Photograph of cable armor made of 0.3-mm-diameter steel wires in eight bundles of two wires wound clockwise and eight bundles of nine wires counterclockwise.

solid copper leads. Three leads are used for the phases. The armor consists of 0.3-mm-diameter steel wires in eight bundles of two wires wound clockwise, and eight bundles of nine wires counterclockwise at the pitch of 38 mm and a weave angle of 47° with respect to the cable axis (see Fig. 2). The open area between the nine-wire bundles is 0.8 mm wide. A 6-mm^2 straight bare copper litz is also embedded inside the armor as protective earth (PE) conductor. There is no further metal shield. The fourth lead in the cable is always connected in parallel with the PE litz at the cable ends.

We measured the output voltages and conducted interference produced by the drive. The net transient current of the three phase leads and the common-mode (CM) current through the cable were determined at the drive and the motor end of the cable by Fischer and Fluke current probes. The signals were recorded on digital scopes at each end (LeCroy and Tektronix); the triggers were synchronized by an optical fiber unit.

The model is based on a multiconductor transmission line (MTL) approach presented in [4]. The transmission line (TL) that acts as source for the disturbances is composed of the three phase leads regarded as bundled single conductor and the armor plus PE and fourth lead regarded as return. The characteristic impedance and propagation speed of the internal TL were measured in the laboratory up to 10 MHz, as is to be discussed in Section IV. The measurements also provided the transfer impedance Z_t of the cable armor between the internal TL and a dedicated external circuit. At Dongemond, the external circuit comprises the soil and the other cables in the trench, and we choose the source cable armor as common return. The excitation is distributed over the source cable length and occurs via the armor Z_t. We did not separately measure the soil properties like the conductivity σ_s, input for the determination of the parameters of the external circuit. First, $\sigma_s = 10^{-2}$ S/m is a representative value for the wet soil in the western part of The Netherlands. The water table strongly influences the effective conductivity; it is maintained constant by the controlled drainage of the lands by mills. The cables lay at constant depth, except for a few meters at the ends. Second, σ_s enters the parameters as argument of a logarithm and little error is introduced by deviations from the actual σ_s. Third, the other cables in the trench are in parallel with the soil and take their share of the external current. These facts induce us to use constant TL parameters over the full length of the investigated cable. The ends are discussed in more detail in Section VII.

The goal of the investigation is threefold. First, we want to determine the disturbance levels in this installation. Second, we want to compare measurements with a model calculation. The model encounters several difficulties since several necessary details such as cable path or terminating impedances are only partially known. In addition, not all metal can be correctly included in the model, for instance, reinforcement grids and bars of unknown interconnection. As a result, one has to make "educated guesses" about their influence. The final goal of this experiment is to find out to what accuracy such estimates can serve to predict the coupling of interference originating in the drives to their environment in spite of the uncertainties.

II. Choice of the Various Current Loops

The circuits for the intended motor currents consist of the voltage sources U, V, and W in the drive, the three leads in the cable, and the three phase-windings of the motor (see Fig. 3). These three currents are well balanced during the major part of the 3-kHz switching waveform, or in other terms for low frequencies. Long cables have large capacitances, which are to be charged/discharged by the drive output. Above a certain cable length, the manufacturer asks for a three-phase choke (see Fig. 3) to avoid activation of the internal overcurrent protection circuit or to protect the drive against current surges. If a current flows through one of the leads and returns through the other two, the magnetic circuit closes in the core of the choke. The corresponding inductance is typically about 1 mH, as has been found by measurement. An unbalance in the three currents comprises a net current equally distributed over the three coil windings. The corresponding magnetic circuit closes via the large air gap of the choke surroundings (see Section VI for details). The unbalance occurs each time when one of the phases in the drive switches over between the negative and positive rail voltage. The average voltage of the three phases changes, and thus, the charge on the cable capacitances. The net current has microsecond-steep rise and fall edges, and is more intense when two phases switch simultaneously in the same direction, or when there is a jitter between phases in switching in opposite direction. Looking at the cable only, the return of this net current is the fourth lead in parallel with the PE litz and the cable armor.

For the analysis of this paper, we then distinguish three current paths in the cable and its environment (see Fig. 4): 0) the armor with the PE litz and the fourth lead; 1) the three-phase leads considered as a bundle; and 2) the soil with the other cables embedded. The choice of 1) is allowed, since the dominant interference is caused by the net current through the three phase leads. The three paths give two independent loops; transmission line TL1 comprises 1) and 0), whereas TL2 is made of 2) and 0). Instead of the usual choice of the soil, we have chosen 0) as the common return. TL1 is terminated at the source end by the coil $U2$, $V2$, and $W2$ outputs bundled as single "hot" terminal and the local ground as "cold" terminal. At the load end one finds the capacitances between the motor windings

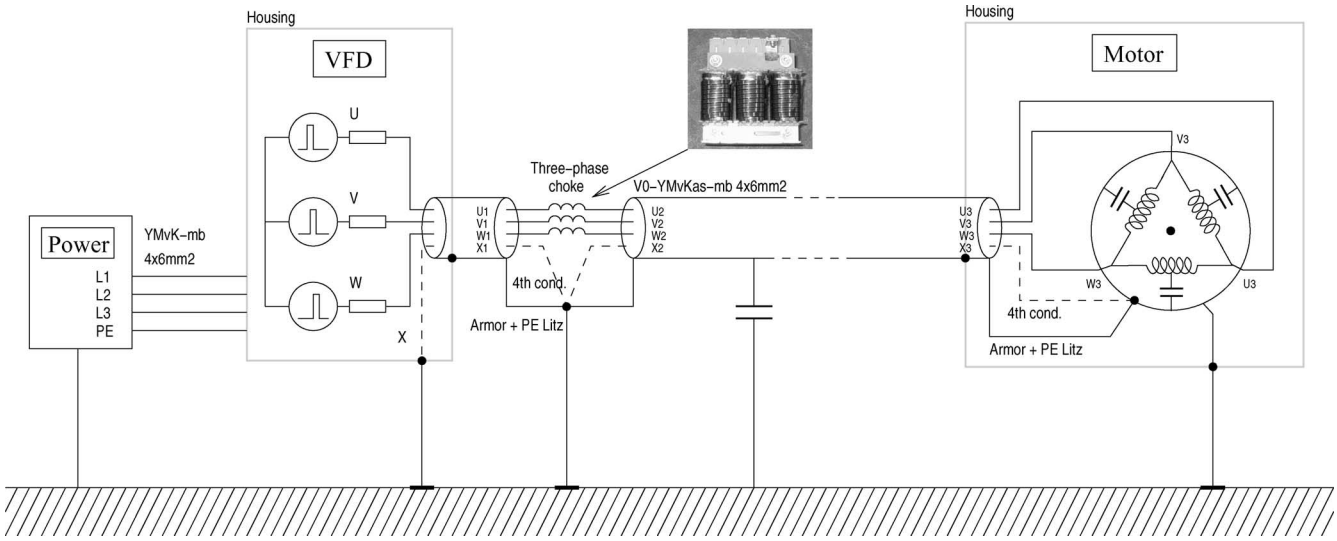

Fig. 3. Setup of the installation. The inset is a photograph of the three-phase choke of the kind used in the installation.

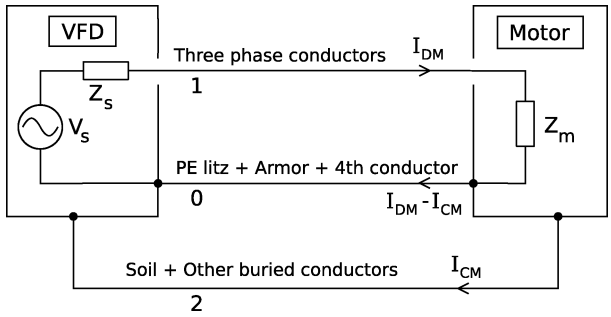

Fig. 4. CM and DM currents.

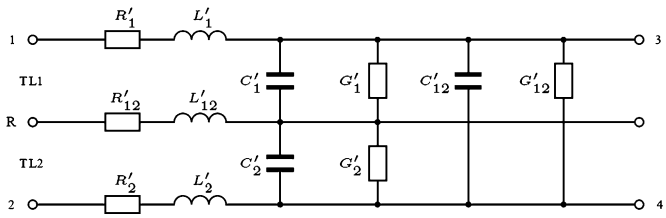

Fig. 5. Infinitesimal transmission line part. TL1 is the bundle of three inner conductors and return is the armor with the fourth conductor and PE litz. Here, TL2 represents the soil and all other parallel cables.

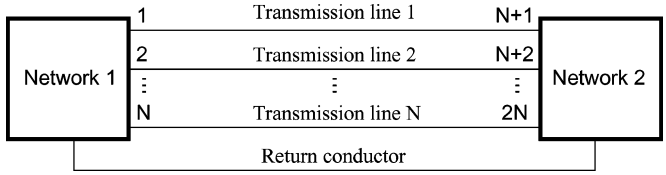

Fig. 6. Model of the setup consisting of an N-conductor transmission line and two terminating networks, with node points numbered.

and its chassis. Borrowing from common EMC language, one may consider TL1, source, and load as the differential-mode (DM) circuit with loop current $I_{\rm DM}$. TL2 is then the CM circuit. This name also indicates that the current in that loop is the algebraic sum of the currents through all conductors of the cable under discussion. A current probe around that cable will measure $I_{\rm CM}$. The coupling between DM and CM circuit occurs via the transfer impedance, where we assume that the cable contribution is dominant. Although it is certainly important in the practical control room [5], we neglect in our model the CM current through other cables toward the drive, for instance, the ac power leads.

Fig. 4 shows a low-frequency model. For frequencies where wavelength becomes comparable to the length, a transmission-line model can be applied to take finite travel times into account.

III. Multiconductor Transmission-Line Approach

As mentioned in Section II, we consider the parallel combination of armor, PE litz, and fourth lead as the reference conductor; it carries the current $I_{\rm CM} - I_{\rm DM}$. An infinitesimal section of the MTL is shown in the coupling model of Fig. 5, where only TL2 has been drawn. The quantities R'_x, L'_x, G'_x, and C'_x are the per-unit-length transmission-line parameters of TL$_x$. The coupling between TL1 and TL2 is represented by the circuit elements R'_{12}, L'_{12}, G'_{12}, and C'_{12}. The real and imaginary parts of the transfer impedance are described by R'_{12} and L'_{12}; both depend on frequency because of the skin effect.

In the actual MTL calculations, we split the soil and the other cables and described them as individual TLs, numbered TL2 for the soil and up to TLN in Fig. 6. Network 1 describes the drive and choke, and network 2 the motor. Both networks contain the connection to the return conductor.

We followed the approach of [4] to calculate the TL voltages and currents. The frequency response of the circuit is derived by assuming a 1-V sine wave voltage source at node 1 and calculating all voltages and currents at the frequencies of interest. The sample frequency used is 1.5 MHz and the number of samples is 256. The DM voltage generated by the drive is sampled and converted to frequency domain via fast Fourier transform (FFT), multiplied by the frequency response of the circuit, and finally, transformed back to the time domain via inverse FFT (IFFT).

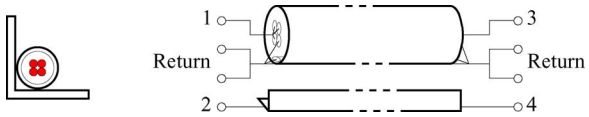

Fig. 7. Setup to determine the transmission line parameters. (Left) Cross-section of the setup. (Right) Schematic representation; the numbers refer to the nodes in Fig. 6.

TABLE I
TRANSMISSION LINE PARAMETERS DERIVED BY CURVE FITTING OF S-PARAMETERS

Parameter	DM circuit (TL1)	CM circuit (TL2)
Z_0	18.5 Ω	23.3 Ω
v	$1.70 \cdot 10^8 m/s$	$2.15 \cdot 10^8 m/s$
$\tan(\delta)$	$10.2 \cdot 10^{-3}$	$24.2 \cdot 10^{-3}$
L'	127 nH/m	119 nH/m
C'	370 pF/m	220 pF/m

IV. MEASUREMENT OF CABLE TL PARAMETERS

A 3.8-m-long cable segment was tested in the laboratory. The cable was pressed in the corner of an aluminum L-shaped bar (see Fig. 7). The setup has two transmission lines: the inner circuit with three leads in parallel and the armor plus fourth lead and PE litz as return, and the outer consisting of the L and the return just mentioned. For both circuits, we derived the transmission line parameters from the S-parameters measured with a vector network analyzer (VNA) consisting of an HP 4396A in combination with an S-parameter set HP 85046A. We limited the frequency band to 10 MHz. For the inner circuit or the cable itself, the reflection parameters S_{11} and S_{22} at the ports formed by nodes 1 and 3 were fitted to the following expressions [6]:

$$S_{11} = S_{22} = \frac{(\bar{Z}_0^2 - 1)\sinh(\gamma l)}{2\bar{Z}_0 \cosh(\gamma l) + (\bar{Z}_0^2 + 1)\sinh(\gamma l)} \quad (1)$$

where $\bar{Z}_0$ is the normalized characteristic impedance, which is $Z_0/50$, and γ is the propagation constant given by

$$\gamma = \alpha + j\beta = \sqrt{(R' + j\omega L')(G' + j\omega C')}. \quad (2)$$

Similarly, the transmission parameters S_{12} and S_{21} from node 1 to 3 and vice versa were fitted to

$$S_{21} = S_{12} = \frac{2\bar{Z}_0}{2\bar{Z}_0 \cosh(\gamma l) + (\bar{Z}_0^2 + 1)\sinh(\gamma l)}. \quad (3)$$

During these measurements, the outer circuit was terminated at both ends into 50 Ω in order to reduce resonances. The same procedure is repeated for the outer circuit on nodes 2 and 4, with the inner circuit terminated into 50 Ω. In this approach, the coupling between the two circuits via the transfer impedance is neglected. The resulting TL parameters are given in Table I as characteristic impedance Z_0, propagation velocity v, and $\tan\,\delta$ for the damping. These parameters can be easily converted to the circuit parameters of Fig. 5. Please note that the parameters of the CM circuit (TL2) obtained here are different from the parameters in the actual installation with the cables in the soil.

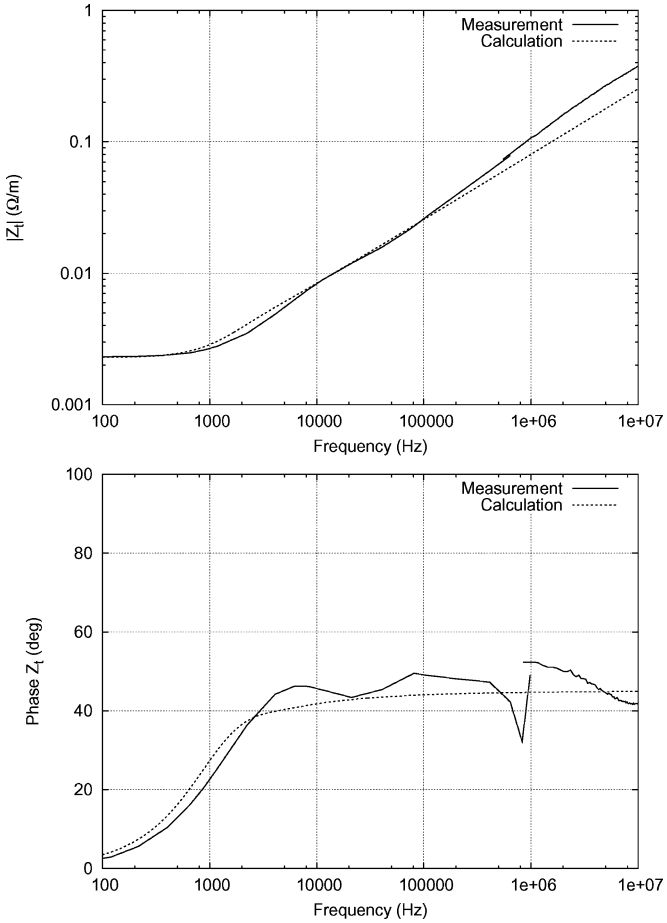

Fig. 8. Measured amplitude and phase of the transfer impedance Z_t'. Below 100 Hz, the phase rapidly tends to zero°. The graphs also show the Z_t' calculated from the fit to the low-frequency data, extrapolated to 10 MHz.

A. Transfer Parameters

The transfer impedance was obtained on a 1.2-m cable segment mounted in a similar L-shaped bar. Between 100 Hz and 1 MHz, a sine wave generator (50-Ω output) provided the current in one TL. The near-end voltage induced in the other TL was measured by a lock-in detector over a 50-Ω termination; the far end of that TL was shorted. The resulting transfer impedance per meter length Z_t' is shown in Fig. 8. Guided by the observed behavior as a function of frequency, we fitted the $|Z_t'|$ to the expression of the surface impedance Z_s' of a single equivalent round wire [7]

$$Z_s'(x) = R_0' \frac{xJ_0(x)}{2J_1(x)} \quad (4)$$

with R_0' being the dc resistance of the wire and $x = \sqrt{-jf/f_\delta}$. Since the frequency variation of Z_s' only depends on R_0' and f/f_δ, we do not specify the wire parameters further. However, for a single round wire of radius a, conductivity σ, and magnetic permeability μ, one would have $R_0' = 1/\pi a^2 \sigma$. At the frequency f_δ, the skin depth $\delta = \sqrt{2/\omega\mu\sigma}$ would be equal to a. The fitted parameters are $R_0' = 2.29$ mΩ$/m$ and the frequency $f_\delta =$ 410 Hz. The lower part of Fig. 8 shows that the calculated phase

of Z'_s is also in good agreement with the measurements. Below 410 Hz, the transfer impedance is about constant as determined by the parallel resistance of the PE litz, the fourth lead, and the armor (1.3 mΩ). In this measurement setup, the contact resistance of the connectors for the armor and PE litz add to R_0. Above 1 kHz, the transfer impedance becomes proportional to the square root of the frequency, indicating a dominant surface skin effect. The near to constant phase angle of Z'_t, which is equal to $\pi/4$ in good approximation, agrees with this interpretation. The low value of f_δ indicates the predominance of the ferromagnetic armor in Z'_t. At frequencies between 300 kHz and 10 MHz, Z'_t has been determined with the VNA. In the region of overlap with the lower frequency data, good agreement is observed. With open-circuit terminations of inner and outer TL, the transfer admittance Y'_t has been determined. Below 10 MHz, $Y'_t = j\omega C'_{12}$ holds with $C'_{12} = 0.23$ pF/m. With this low capacitance value, the coupling via Z'_t dominates the Y'_t contribution over the frequency range of interest. As a test, the measured Z'_t was used to calculate the transfer between both TLs in the setup with the 3.8-m-long aluminum L-shaped bar. Good agreement was obtained.

V. Modeling Soil and Other Buried Cables

As mentioned in Section III, the soil is modeled as TL2 and the other buried cables as TL3–TLN. We now present equations for the transmission line parameters in the form of per-unit-length impedance (Z' in Ohms per meters) and admittance (Y' in siemens per meter).

A. TL2

TL2 consists of the soil surrounding the cable as forward conductor and the armor of the cable as return conductor, separated by the polyvinyl chloride (PVC) insulation of the cable. Expressions for the impedance and admittance of such a transmission line can be found in [8]. The impedance consists of the internal impedance of the soil Z'_g, the internal impedance of the armor Z'_i, and the inductive reactance $j\omega L'$ of the space occupied by the cable's outer insulation. The internal impedance of the soil can be expressed analogous to (4) as

$$Z'_g = R'_s \frac{x_s K_0(x_s)}{2K_1(x_s)} \tag{5}$$

(see, e.g., [9] and [10]). Here, $x_s = \gamma_s r_b$ and $\gamma_s = \sqrt{j\omega\mu_s(\sigma_s + j\omega\epsilon_s)}$ is the propagation constant for a soil with conductivity σ_s, magnetic permeability μ_s, and electric permittivity ϵ_s. $R'_s = 1/\pi r_b^2 \sigma_s$ stands for the resistance per meter soil over the volume excluded by the cable. The outer radius of the cable including the insulation is r_b.

As mentioned in Section I, the armor of the cable consists of 8×11 parallel steel wires with a radius $r_{\rm sw} = 0.15$ mm (see Fig. 2). The pitch of the steel wire spiral is 38 mm. Combined with a radius of the armor $r_a = 6.5$ mm, the total length of steel wire per spiral turn is 56 mm. If we neglect the interaction between neighboring wires, the internal impedance is

$$Z'_i = \frac{1}{8 \cdot 11} \frac{56}{38} Z'_s(x_{\rm sw}) \tag{6}$$

with $Z'_s(x_{\rm sw})$ as in (4) with the parameters of the steel wires. Again, the ferromagnetic properties of the steel strongly increase Z'_i over a nonmagnetic material like copper.

The self-inductance of the space occupied by the cable outer PVC insulation is straightforward

$$L' = \frac{\mu_0}{2\pi} \ln\left(\frac{r_b}{r_a}\right). \tag{7}$$

The total admittance is the series connection of the capacitance of the insulation gap and the admittance of the soil. The capacitance of the cable outer insulation is given by

$$C' = \frac{2\pi\epsilon_i}{\ln\left(\frac{r_b}{r_a}\right)}. \tag{8}$$

In this equation, ϵ_i is the dielectric permittivity of the outer insulating. The admittance of the soil is approximated by

$$Y'_g \approx \frac{\gamma^2}{Z'_g}. \tag{9}$$

The upper part of Fig. 9 shows Z'_g, Z'_i, and $j\omega L'$, and the total series impedance Z'. One notes that the soil contribution, mainly Z'_g, determines Z' above 5 kHz. This crossover frequency would be lower if the PE litz and fourth conductor would contribute to Z'_i. The lower part shows Y'_g and $j\omega C'$ and total Y'. Here, the cable insulation dominates in Y' over the frequency region of interest, i.e., below 750 kHz.

B. TL3–N

The impedance of these TLs consists of twice the Z'_g of the cable in the soil (5) and twice the Z'_i of (6). The additional coupling between the cables via the magnetic field in the soil can be expressed by a mutual impedance M' in $-2j\omega M'$. We followed the approach of [11, eq. (4.44)]

$$M' = \frac{\mu}{2\pi}[K_0(\gamma d) - K_0(\gamma d_i) + W(\gamma d_i)] \tag{10}$$

where

$$W(\gamma d_i) = 2\int_0^\infty \frac{e^{-2z\alpha}\cos(ud)}{\alpha + u} du. \tag{11}$$

In this equation, d is the distance between the cables, $\alpha^2 = \gamma_s^2 + u^2$, and $d_i = \sqrt{d^2 + 4z^2}$, where z is the burial depth of the cables. Please note the change in variables with respect to [11]. We used $d = 2$ cm and $z = 1$ m. The integration of (11) has been carried out numerically up to an upper boundary $u = 10$. If we increased the upper boundary from $u = 10$ to $u = 100$, the relative change in W was 10^{-8}, indicating sufficient convergence.

C. Coupling Between TL2 and Other Buried Cables

The coupling between TL2 and a nearby buried cable is a coupling of the electromagnetic fields in the soil (TL2) to the armor of another cable. This coupling is comparable to the coupling of lightning-induced fields in the ground to buried cables, which is described in [12]. Their model is valid until 30 MHz, which is far beyond our maximum frequency of

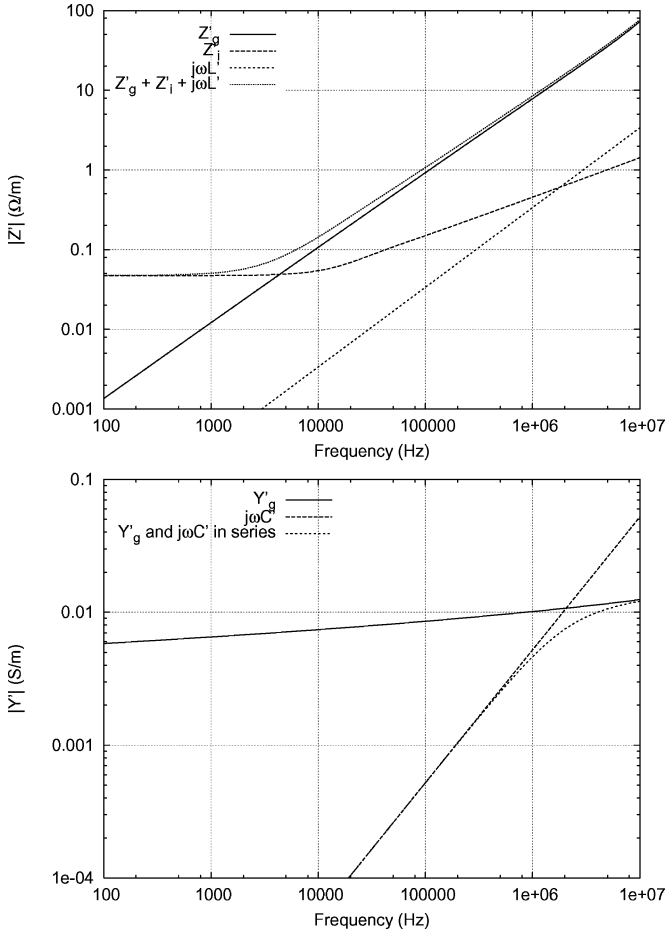

Fig. 9. Contributions to (top) the impedance and (bottom) the admittance by the cable and by the soil. The cable dimensions have been mentioned in the main text. The soil parameters were $\sigma_s = 0.01$ S/m, $\mu_s = \mu_0$, the magnetic permeability of vacuum, and $\epsilon_s = 10\epsilon_0$ with ϵ_0 being the permittivity of vacuum. For the steel wire, we used $\sigma_{\rm sw} = 10^7$ S/m and $\mu = 500\mu_0$, and for the PVC cable insulation, $\epsilon_i = 4\epsilon_0$.

750 kHz, that makes their approach useable in our situation. The buried cable in the ground is modeled as a transmission line with a series voltage source E_z (see Fig. 10). The voltage of this source is equal to the tangential electric field at the location of the cable. The electric field parallel to the cable as a function of the distance to the cable r, generated by the current I in the armor, is given by

$$E_z = \frac{\gamma_s I K_0(\gamma_s r)}{2\pi\sigma_s r_b K_1(\gamma_s r_b)}. \tag{12}$$

As can be derived from Fig. 10, the voltage per meter over the armor of the other buried cable is given by

$$V = \frac{Z_i'}{Z_i' + Z_c'} E_z \tag{13}$$

where

$$Z_c' = Z_g' + j\omega L' + Z_0 + \frac{Z_0(j\omega C' + Y_g')}{Z_0 j\omega C' Y_g' + j\omega C' + Y_g'} \tag{14}$$

and Z_0, Z_i', Z_g', Y_g', L', and C' are equal to the parameters of TL2.

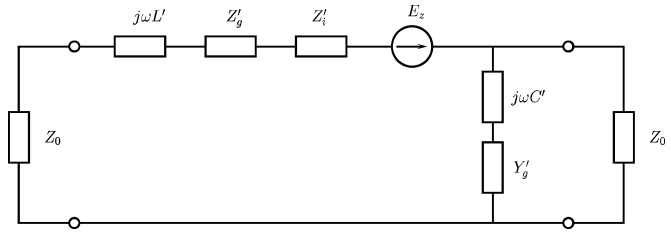

Fig. 10. Infinitesimal part of transmission line formed by a buried cable in the soil.

VI. Simulation Results for the Actual Installation

The DM current primarily depends on the TL1 parameters given before. The coupled inductance of the choke has been determined by interconnecting the three input terminals U1, V1, and W1 at one side and interconnecting the three output terminals U2, V2, and W2 at the other side. The inductance between the "1" and the "2" sides is 4.4 μH over the frequency range of interest, as measured by an Agilent 4263B impedance meter. The internal impedance of the inverter is assumed to be negligible compared to the choke impedance. The motor windings have a capacitance of 4.16 nF with respect to the chassis, as measured for the three phase windings together. With these parameters, the lowest resonance frequency of TL1 and its terminations are in good agreement with the observed 300-kHz ringing found in the measurements (see Fig. 11). At this frequency, the calculated ratio of the DM current at the drive to the DM current at the motor is about a factor of 5, as is also seen in the measurement results presented in Table II. The time-domain DM current has been calculated as the response to a slope-limited voltage step at node 1 (see Figs. 5, 6, and 11). The supply voltage in the drive is 260 V for each polarity. In the selected data, two phases switched simultaneously, which is equivalent to a source voltage at node 1 of $2/3 \times 520 = 347$ V. The calculated DM current peak-to-peak value agrees well with the measurement.

The external TLs are modeled as parallel lines. However, in the actual installation, these are less well known because there are many possible current paths outside the TL1 cable of interest: the soil, other cables, and the concrete reinforcement. To cope with this uncertainty, we compare three situations: 1) TL1 is a single buried cable in the soil with a conductivity σ of 10^{-2} S/m common for wet soil and no other conductors in the neighborhood; 2) the other conductors simulated by an adapted soil conductivity of 50 S/m; and 3) all other cables modeled by a bundle of four. In both cases, we use the approximations for the TL2 impedance and admittance given by Vance [8, Ch. 4], and we assume that TL2 is terminated into a short circuit to the common return at both ends.

In Table II, the following results have been summarized.

1) The simulated time-domain CM current for the common soil is too small by a factor of 150, so the other conductors must be taken into account.
2) The soil conductivity of 50 S/m gives reasonable agreement between the simulated and measured time-domain CM current. Close to the drive, the ratio of the currents in TL1 and TL2 is about a factor of 20. The current ratio at beginning and end of TL2 is about 2.5.

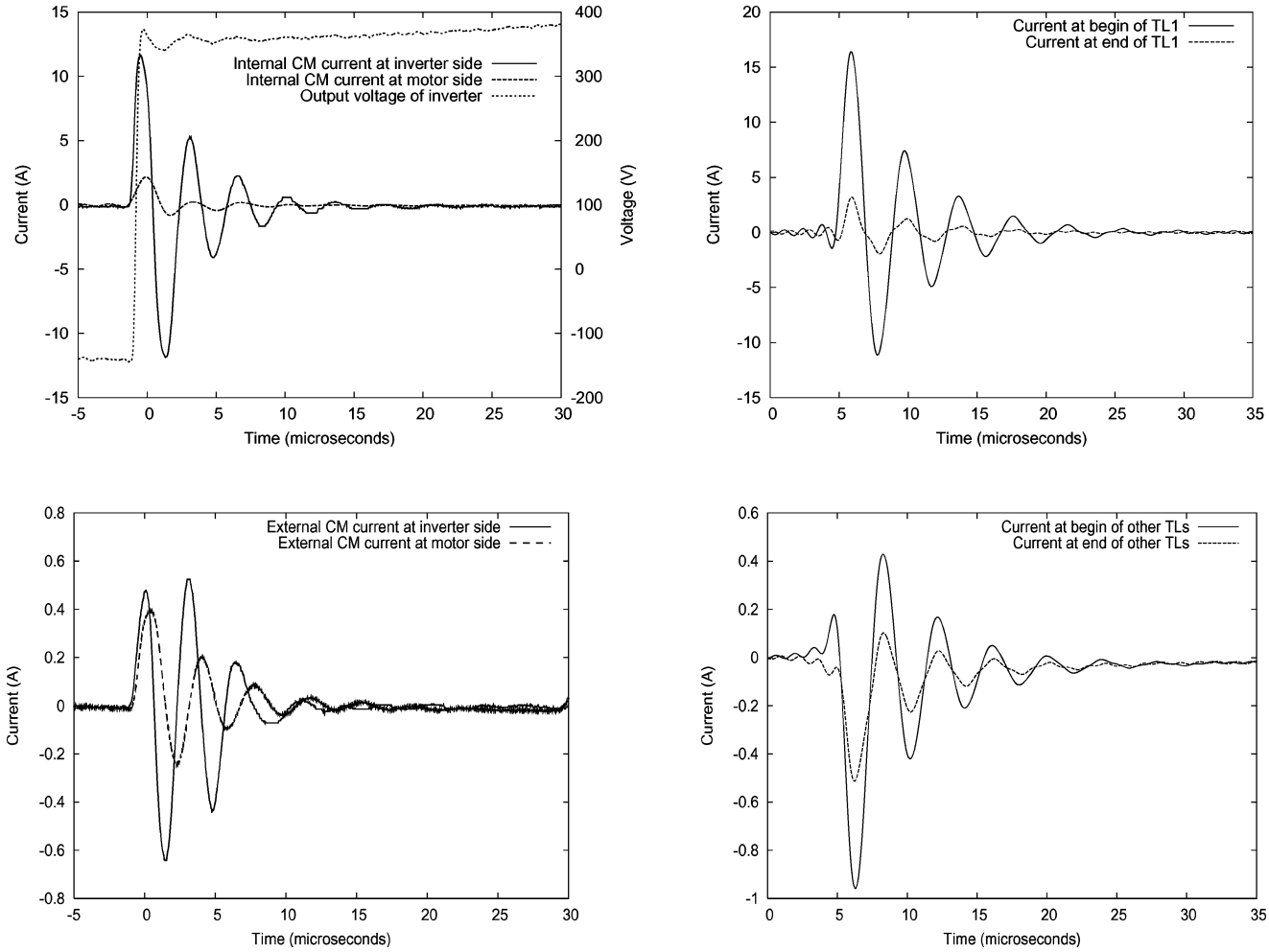

Fig. 11. Time-domain result of (left plots) the measurements and (right plots) the calculations. The plots on top give the results for the inner conductors, which is called TL1 in the simulations. The bottom plots give the results of the summation of the currents in all other transmission lines. The voltage step measured on a single phase is shown in the top left plot.

TABLE II
SIMULATED VALUES OF DM AND CM CURRENTS AT INVERTER AND MOTOR SIDE

		simulated			measured
σ (S/m)		10^{-2}	50	10^{-2}	
#other cond. n		0	0	4	
300 kHz	TL1 begin	0.13	0.13	0.13	
	TL1 end	0.019	0.019	0.019	
	TL2-N begin	$1 \cdot 10^{-4}$	$6 \cdot 10^{-3}$	$7 \cdot 10^{-3}$	
	TL2-N end	$1.6 \cdot 10^{-5}$	$2.3 \cdot 10^{-3}$	$1.8 \cdot 10^{-3}$	
time domain	TL1 begin	25	25	26	23.4
	TL1 end	4.5	4.5	5.0	4.9
	TL2-N begin	0.021	1.4	1.5	1.12
	TL2-N end	0.004	0.5	0.6	0.6

The 300-kHz data assume a 1-V excitation at node 1. The simulated time-domain data are the peak-to-peak values for a voltage rise at node 1 of 347 V.

3) If four other cables ($n = 4$) are taken into account (see Fig. 13), the simulated currents are in reasonable agreement with the measured currents. Figs. 11 and 12 present the TL currents for this case.

VII. DISCUSSION

The prominent feature in the measured currents is the 300-kHz ringing frequency. The TL1 cable parameters and 4.16-nF capacitance at the motor end have been measured with an accuracy of the order of 1%. The actual length may vary by about 5% from the 85 m used in the calculation. The 4.4-μH self-inductance of the choke is essential to obtain agreement between measured and calculated resonance frequency and current amplitude.

The other cables are necessary in the model to explain the observed CM current. The second model, which relies on the soil alone, needs an unrealistically high conductivity of 50 S/m.

The other cables in the ground are taken into account by regarding them as additional transmission lines that have the same length and follow the same path as TL1. All other motor drives are placed next to each other in the control kiosk. The motors are all connected to the local grounding which includes the concrete reinforcement. We assumed that this distributed grounding acted as a single connection for the CM current. Further modeling would require detailed information about all connections, which was not available.

As Fig. 1 shows, the many parallel cables form a spaghetti cluster, rather than a strictly parallel set of cables. In principle, a statistical model should have been more adapted to describe

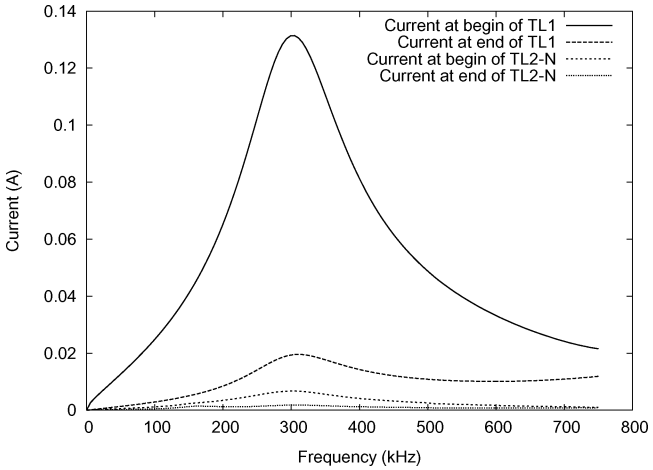

Fig. 12. Frequency-domain result of calculation of the TL currents for 1-V excitation at node 1. The ratio of the current at the beginning of TL1 to the current at the end of TL1 at 300 kHz is about 5. This is the simulation with four other buried conductors.

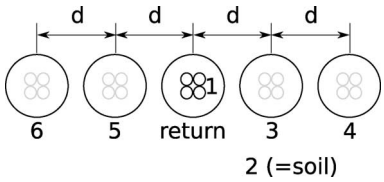

Fig. 13. Arrangement of four other buried conductors. The numbers refer to the transmission-line numbers. The distance d between the cables is 2 cm.

the TL3 and higher. Such models have been proposed (see, e.g., [13]). However, we checked the sensitivity of the calculation results to the number of parallel cables. An increase in the number of cables in our model from 4 to 6 did barely alter the CM current. We did not measure the individual CM currents through the other cables.

The accuracy of the soil parameters is less important, because the soils carry only a small current and because these parameters enter the calculations primarily as part of the argument of a logarithm.

The four leads of the TL1 cable are positioned in a square arrangement. The symmetry is reflected in the current–voltage patterns of the four normal transmission modes. The PE litz inside the shield then destroys the precise fourfold symmetry of the configuration, complicating the mode patterns. Slight differences in propagation speed and damping between the modes might be expected. We therefore measured the effective TL parameters with the cable connected as in the practical situation: three phase leads bundled and the fourth lead grounded to PE litz and armor. Over the frequency band below 1 MHz, the differences in mode propagation are not important. If the measurement and modeling would be extended to higher frequencies, such differences would certainly have to be accounted for. The measurements were performed with 8-bit resolution. The spectra did not show sufficiently clear high-frequency features to warrant a detailed analysis.

The transfer impedance Z_t' has been measured in the same configuration, three leads combined, and the fourth lead plus PE litz connected to the shield at the ends. It is to be expected that the Z_t' depends on the shape of the outer return and the position of PE litz with respect to the external conductor. Also, the position of the fourth lead varies over the length since the inner leads spiral around the cable axis. We checked the variation of Z_t' with the L-shaped bar (Section IV) replaced by a 20-cm-wide copper foil at a few distances up to 5 cm, and with the cable rotated over its axes. The Z_t' values remained within 15% equal to the data of Fig 8.

With its total coupled inductance of 4.4 μH, the choke is not very effective to reduce the net current through the three phase leads. Another approach makes a more effective use of the fourth lead: install a balancing transformer with four windings on a single yoke with the magnetic circuit closed. Such a transformer forces the net current through the three phase leads to return through the fourth lead. This approach relieves the requirements on the armor or a shield, but does not necessarily make these superfluous. The transformer has indeed been used in a practical situation [14] with good result.

VIII. Conclusion

The results of a field measurement in a complex industrial installation have been presented. A careful connection of a steel armor—as if it was a high-quality shield—reduces the interference by about a factor of 20 (95% of the disturbing current is flowing back in this shield, instead of in other cables).

The calculated DM and CM currents agree well with the measurements. The armor of the neighboring cables provide a low-impedance path for the CM currents. The soil is less important as CM return in this installation.

In the model, the other buried conductors are short-circuited to the return conductor at the beginning and end of the TLs. This appears to be a good approximation although in reality the other TLs are longer than the one under consideration.

Acknowledgment

This work has been carried out in a cooperation between the Universities of Technology in Eindhoven and in Delft. A. P. Pratomo participated in the measurements. The support of M. Schapendonk and E. van Seumeren (GTI, The Netherlands) and H. Maas (Brabants Delta, The Netherlands) during the preparation of the measurements is gratefully acknowledged. Ir. G. Bargboer carried out some of the Z_t' measurements. The authors thank her for her assistance.

References

[1] IOP ElektroMagenetische VermogensTechniek (EMVT). [Online]. Available: www.senternovem.nl/iopemvt/algemeen/index.asp

[2] NEN 3207, "Insulated power cables and flexible cords. Systems for the designation of types of cables," Nederlands Normalisatie Inst., Delft, The Netherlands, 1990.

[3] *Installation and mitigation guidelines, section 2: Earthing and cabling*, IEC Standard 61000-5-2, 1997.

[4] A. R. Djordjević and T. K. Sarkar, "Analysis of time response of lossy multiconductor transmission line networks," *IEEE Trans. Microw. Theory Tech.*, vol. MTT-35, pp. 898–908, Oct. 1987.

[5] D. Zhao, J. A. Ferreira, H. Polinder, A. Roch, and F. B. J. Leferink, "Noise propagation path identification of variable speed drive in time domain via

common mode test mode," in *Proc. Power Electron. Appl. Conf.*, Sep. 2007, pp. 1–8.
[6] P. A. Rizzi, *Microwave Engineering, Passive Circuits*. Englewood Cliffs, NJ: Prentice-Hall, 1988.
[7] S. Ramo, J. R. Whinnery, and T. van Duzer, *Fields and Waves in Communication Electronics*, 2nd ed. Chichester, U.K.: Wiley, 1984.
[8] E. F. Vance, *Coupling to Shielded Cables*. Hoboken, NJ: Wiley, 1978.
[9] P. C. Magnusson, G. C. Alexander, V. K. Tripathi, and A. Weisshaar, *Transmission Lines and Wave Propagation*, 4th ed. Boca Raton, FL: CRC, 2001.
[10] R. V. Langmuir, *Electromagnetic Fields and Waves*, 1st ed. New York: McGraw-Hill, 1961.
[11] E. D. Sunde, *Earth Conduction Effects in Transmission Systems*, Dover ed. New York: Dover, 1968.
[12] E. Petrache, F. Rachidi, M. Paolone, C. A. Nucci, V. A. Rakov, and M. A. Uman, "Lightning induced disturbances in buried cables—Part I: Theory," *IEEE Trans. Electromagn. Compat.*, vol. 57, no. 3, pp. 498–508, Aug. 2005.
[13] D. Bellan and S. A. Pignari, "Estimation of crosstalk in nonuniform cable bundles," in *Proc. IEEE Int. Symp. Electromagn. Compat.*, Chicago, IL, Aug. 2005, vol. 2, pp. 336–341.
[14] M. J. Coenen, EMCMCC, Eindhoven, The Netherlands, private communication.

H. Tjerk Steenstra received the M.Sc. degree in electrical engineering from the Delft University of Technology, Delft, The Netherlands, in 1998.

Since 1998, he was a Researcher at the International Research Centre for Telecommunications, Transmission, and Radar, where he worked on the processing of a multistatic frequency-modulated continuous wave radar for collision avoidance purposes. In 2003, he shifted to the HV Technology and Management Group, Delft University of Technology, where he worked on the EMC of cabling and wiring in buildings and installations, in cooperation with the University of Technology in Eindhoven, The Netherlands. He is currently with Mapper Lithography, Delft.

Alexander P. J. van Deursen (A'97–SM'97) received the Ph.D. degree in physics from Radboud University, Nijmegen, The Netherlands, in 1976.

He was a Postdoctoral Researcher at the Max Planck Institut fur Festkorperforschung, Hochfeld Magnetlabor, Grenoble (France). He returned to Nijmegen, where he worked on solid-state physics on electronic structures of metals, alloys, and semiconductors by high magnetic field techniques. In 1986, he joined the Eindhoven University of Technology, Eindhoven, The Netherlands, where he has been engaged in electromagnetic compatibility (EMC). He has also been engaged in several International Electrotechnical Commission's (IEC) working groups.

Dr. van Deursen has been the Chairman and member of different committees in international conferences. He is also a member of the International Council on Large Electric Systems (CIGRE) SC36, the European Committee for Electrotechnical Standardization (CENELEC), and the International Steering Committee of EMC Europe.